Low-cost plastic optical fiber integrated with smartphone for human physiological monitoring

Renfei Kuang[1], Yifan Ye[1], Ziyang Chen[1], Runjie He[1], Isidora Savović[2], Alexandar Djordjevich[3], Svetislav Savović[4], Beatriz Ortega[5], Carlos Marques[6], Xiaoli Li[1] and Rui Min[1]*

[1]*Center for Cognition and Neuroergonomics, State Key Laboratory of Cognitive Neuroscience and Learning, Beijing Normal University, 519087 Zhuhai, China*
[2]*School of Biomedical Sciences, LKS Faculty of Medicine, Laboratory of Neurodegenerative Disease, Department of Mechanical Engineering, The University of Hong Kong, Hong Kong, China*
[3]*City University of Hong Kong, 83 Tat Chee Avenue, Kowloon, Hong Kong, China*
[4] *Faculty of Science, University of Kragujevac, R. Domanovića 12, 34000 Kragujevac, Serbia*
[5] *ITEAM Research Institute, Universitat Politècnica de València, 46022 Valencia, Spain*
[6] *I3N & Physics Department, Universidade de Aveiro, 3810-193 Aveiro, Portugal*
* *Corresponding: ruimin@bnu.edu.cn*

Abstract:

Human physiological signal monitoring is a key factor in diagnosing health conditions, such as monitoring heart rate and respiration. To meet the increasing monitoring requirements, such as safety, economy, and equipment miniaturization, it is necessary to optimize and improve the monitoring device. Polymer optical fiber sensor has great potential in human physiological monitoring because of their inherent safety, compactness, electrical isolation, and flexibility. In this paper, we report the integration of low-cost plastic optical fibers in smartphones for the measurement of respiratory rate and heart rate in human physiological monitoring. The performance of the plastic optical fiber (POF) sensor with different sensitivity zone is analyzed. With three sensitivity zones, the respiratory rate and heart rate can be displayed in the power spectral density simultaneously. For improving the POF sensor performance, the shutter speed of the smartphone is also optimized to 30 s^{-1}. Finally, the POF sensor is tested under different motion states indicate that the sensor can monitor the heart rate and breathing rate under different postures (running, walking, standing, squatting and lying), where the spectral energy is $2.8 \pm 0.11 \times 10^8$ pt during running and is $1.4 \pm 0.55 \times 10^7$ pt in the supine state. And it also can be used to assess the dynamic posture, which is important for some potential sensory applications in clinical and home settings.

1. Introduction

Human physiological signs such as heart rate (HR) and respiration (breathing) rate (BR) are the key elements in the diagnosis of health conditions and abnormal situations such as bradycardia, tachycardia, hypoxemia, and tachypnea [1]. Among different types of sensors that can be used to obtain the physiological signs data, electronic sensors are the main solutions for monitoring physiological signs at this moment [2]. However, electrical safety issues, electromagnetic interference and the narrow linear time response interval are some of their main disadvantages.

In recent years, optical fiber sensing and information network technologies have undergone rapid development [3-5]. Typically, silica optical fibers are employed for sensing applications due

to the low attenuation, lightweight and immunity to electromagnetic interference [6]. However, for some specific sensing scenarios such as wearable devices on the human body, sensors based on silica fibers have some drawbacks related to its low flexibility, hardness and shattering capabilities, which could damage the human body [7-9]. Also, the price of demodulating equipment for sensors based on silica optical fiber is quite high. Therefore, sensors with high flexibility and low-cost demodulation are required for physiological signs monitoring.

Polymer optical fibers (POFs) are fibers made of plastic materials, such as poly(methylmethacrylate) (PMMA) [10-11], TOPAS [12-13], ZEONEX [14-15], and CYTOP [16-17]. Besides some of the benefits shown by silica fibers, they have some specific advantages, i.e.high flexibility and low-cost demodulation [18-20]. POF sensors for physiological signs monitoring are promising, such as *Han et al.* reported sensors embedded in mattresses to measure HR and BR with the aim of sleep performance monitoring [21] in different postures and positions. However, such low cost system required reliable cutting POF technology and also, an electrical circuit for demodulation. Another example presented by *Leal-Junior et al.* employed side polish technology for measuring HR and BR, and was embedded as a smart textile [22]. The experiment results indicate errors below 4 beats per minute and 2 breaths per minute for the HR and BR, respectively, even when the user is performing periodic body movements such as the ones induced by the gait. However, for the sake of decreasing the demodulation devices, one promising solution is to integrate a POF sensor with a smartphone where the flashlight and camera are used as light source and detector, respectively. *Aitkulov et al.* reported a POF sensor integrated with a smartphone for breath monitoring based on displacement modulation [23]. Since unaltered POF does not have sufficient sensitivity for bending, this an attractive multiplexing concept based on “camera-division multiplexing” was proposed and implemented [24].

In this paper, we report the integration of a low-cost POF and a smartphone for human physiological monitoring. The proposed device is able to measure BR and HR, with the simplicity and low cost as their main advantages, compared with other existing devices. The performance of the POF sensors is analyzed in detail and has been improved by using multiple sensitivity zones. Also, the shutter speed of the smartphone is optimized to improve performance. The POF sensor is tested for measurement in different motion states and the results indicate that BR and HR can be correctly monitored under running, walking, standing, sitting, and lying. Moreover, the dynamic posture can be judged by the sensor system. The paper is structured as follows: Section 2 presents the sensor design, fabrication, and principle; Section 3 main focuses on data processing, such as acquiring the pixel data from the camera of the smartphone and analyzing HR and BR from the pixel value per frame; Then, section 4 present the experimental results, such as analyzing HR and BR with different sensitivity zone, optimizing the parameter of the smartphone, and analyzing HR and BR with different postures.

2. POF-smartphone sensor design

2.1. Overall system design

The schematic of the full system as Fig. 1 shows, can be divided into three main parts: light-generating and receiving device (smartphone), POF-based device, and data processing part. The optical signal generating and receiving device is composed of a smartphone flash, camera, and optical fiber connector. Both light source (flashlight) and optical signal receiver (camera) are

integrated by the smartphone, and the optical fiber connector is completed by 3D printing. The POF-based device consists of POF with a sensitivity area. The sensor is wrapped in three circles around the user's chest, and the sensing zone is aligned at the participant's left chest where the heartbeat is the strongest. Breathing and heartbeat cause the sensor to bend slightly, regulating the amount of light leakage from the sensitivity zone. Subsequently, breathing videos are collected by the camera, and finally, the BR and HR are extracted using a computer program algorithm.

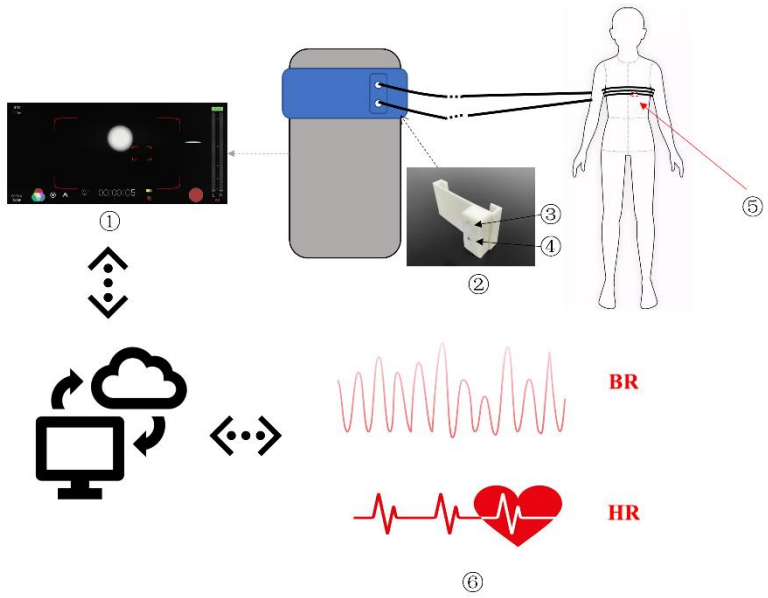

Fig. 1. Schematic diagram of the overall design (①Screenshot while recording video ②Photo of 3D connector ③Camera hole ④Flashlight hole ⑤POF sensitivity zone ⑥Extraction of BR and HR).

2.2. 3D Connector design

To avoid the light from the outside, a 3D-printed connector was designed for POF to connect to the smartphone flashlight and camera. The 3D-printed connector as Fig. 2 shows, was designed with the Pro/E software. Then 3D printing with the 3D printer (Creality CR-3040 Pro) uses PLA as the printing material and chooses 80% infill [25]. The connector fits the smartphone where its flashlight and camera are aligned with the position of POF to avoid the disturbance by ambient stray light. Furthermore, the connector is designed with a 15 mm depth away with the light-receiving position to keep the POF further away from the camera, in order to perceive optical signal power changes.

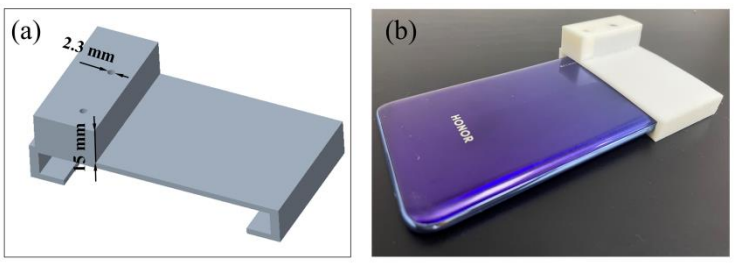

Fig. 2. (a) 3D connector model; (b) Photo of the connector with smartphone.

2.3. POF sensing principle

The schematic diagram of light transmission at the sensing zone is shown in Fig. 3. POF is partially cut at the sensing zone resulting into optical radiation loss. Due to human breathing and heartbeat, pressure is exerted on POF. As a result, the POF wrapped around the chest is slightly bent. It caused optical leakage increases at the sensitivity zone and thus optical signal power change allows to sense the breathing and pulse induced motions.

Optical power attenuation in the sensing zone can be estimated by geometrical optics. The longitudinal section of the POF in the sensing zone is taken for modelling. In this case, the ratio of the output optical signal power (P_o) to input optical signal power (P_i) is defined as relative losses (L_R)[26]:

$$L_R = \frac{P_i - P_o}{P_i} = \frac{2I_i\theta - I_o\beta}{2I_i\theta} \tag{1}$$

where β is the opening angle of the effective received area, I is a constant (i,e. $I_o = I_i$), θ is the critical angle, which satisfies: $sin\theta = \frac{NA}{n_{co}}$. The numerical aperture (NA) of a POF is 0.47, and the refractive index of the core (n_{co}) is 1.49. Considering that the power loss of the optical power increases as the cutting depth increases, but it also leads to more fragility of the sensor, the perpendicular cutting depth is set to be 2/3 of the fiber core diameter. [27]. As shown in Fig. 3(b), D is the fiber core diameter, α is the opening angle of the POF sensing zone. When α is 0, there is no optical power leakage (Fig. 3(a)). Breathing causes the opening angle α to change. From the cosine theorem within the geometrical optics, the following equations can be obtained:

$$\cos(\alpha+\gamma) = \frac{(\frac{2}{3}D)^2 + d^2 - x^2}{2\cdot\frac{2}{3}D\cdot d} \tag{2}$$

Where it can be obtain from the geometric optics that $cos\gamma = \frac{D}{6d}$, $c = \frac{D}{2tan\theta}$, $d^2 = c^2 + (\frac{1}{6}D)^2$.

And x is calculated by the sine theorem within the geometric optics as:

$$\frac{2D}{3x} = \frac{\sin(\beta-\theta_1)}{\sin(\alpha+\gamma)} \tag{3}$$

where $\theta_1 = \theta - \frac{\pi}{2} + \gamma$.

According to Eqs. (1)-(3), the dependent correlation between relative losses (L_R) and opening angle α can be drawn, as shown in Fig. 3(c). The plot verifies the proposed sensing principle is based on the opening angle change within the sensing section.

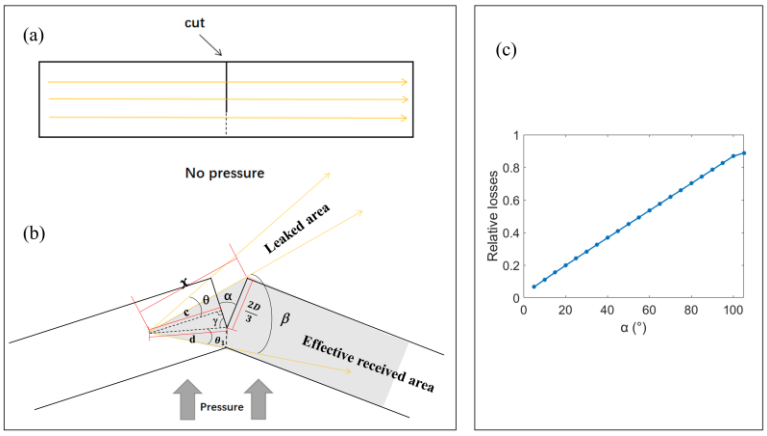

Fig. 3. (a) Propagation of light in a normal condition; (b) longitudinal section view of the sensing zone; (c) Correlation between relative losses and the opening angle.

2.4. POF sensitivity zone fabrication

Choosing an appropriate cutting method to create a sensitivity zone is critical for sensing. As shown in Fig. 4(a), we proposed to cut the fiber cladding and part of the inner core perpendicularly on the surface of fiber with a blade. From the POF sensing principle, the perpendicular cutting depth set to 2/3 of the fiber core diameter is suitable for sensing. The POF used in the experiment is a low-cost plastic optical fiber (Mitsubishi, QY40-2.2E) with a core diameter of 1 mm and an outer diameter of 2.2 mm. To ensure a repeatable and precise cutting, a 3D-printed mold was designed as shown in Fig. 4(b). The mold was printed using 100% fill to ensure the stability of multiple cuts. A channel with the same diameter as the fiber was set to facilitate the fiber to fit the mold [28], Figs. 4(c) and (d) showed the cutting mold and the POF with sensitivity zone after cutting, separately.

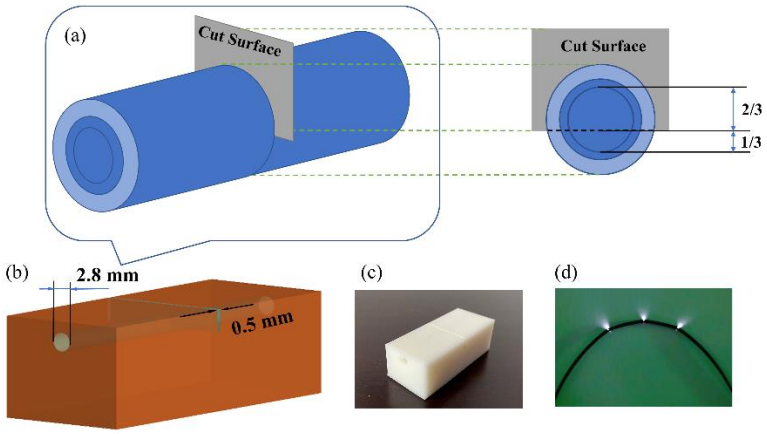

Fig. 4(a) Schematic representation of POF cutting; (b) Model of 3D cutting mold; (c) Photograph of cutting mold;(d) Photograph of POF with sensitivity zone.

3. Data processing principle

3.1. The pixel data acquisition

Data acquisition processing is completely done by the camera of the smartphone (Honor 20i from Huawei). The video is recorded using the third-party application FiLMiC Pro, where the

interface of the video recording process is shown in Fig. 1. Compared to the native camera, the third-party application FiLMiC Pro allows the user to determine various parameters of the video recording process freely. The parameters are fixed during the video recording process as shown in Table 1.

Table 1. Some camera parameters of the video recording process

Shutter speed	Video frame rate	ISO	Video resolution	Aspect Ratio
1/30s	30 FPS	50	540p	16:9

A video is captured by the camera while the participant is breathing normally. Subsequently, the video is outputted frame-by-frame and then the color-to-Grayscale processing is performed on each frame. In a grayscale image, the pixel value is equal to the grayscale value. As shown in Eq. (5), the grayscale values, (i.e, the pixel values) of a single frame, are summed to estimate the optical power received by this frame [23].

$$\text{Optical power} = \sum_{x=1}^{a} \sum_{y=1}^{b} \text{Pixel}_{ab} \tag{5}$$

where x and y represent the plane coordinates of each frame pixel, a and b are both set to 540 since the resolution of each frame of the video recorded by this third-party application is 540×540 pixels.

3.2 Extraction of BR and HR

Normally, the frequency of BR and HR on the different ranges can be extracted by analyzing the spectrum of these two parts respectively. The direct-current (DC) component of the data is eliminated and the power spectrum of optical power is calculated by using Welch's overlapped segment averaging estimator [29].

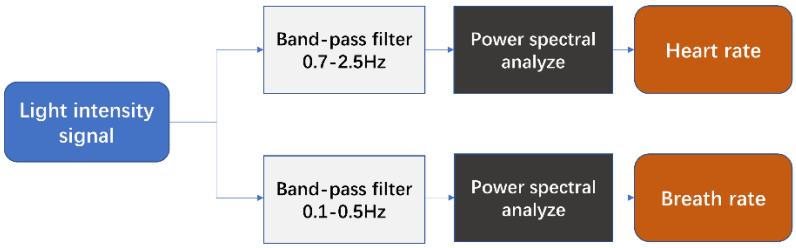

Fig. 5. The process of calculating BR and HR.

The proposed processing steps for extracting BR and HR are shown in Fig. 5. The signal is divided into segments as Eq. (6):

$$x_i(n) = x(n + iM - M), \qquad 0 \le n < M, \qquad 1 \le i < L \tag{6}$$

where M is the length of the window and L denotes the number of data samples segments and i indicates the number of each segment. Then Eqs. (7) - (8) are used to calculate the modified periodograms of each segment in a Hamming window design.

$$I_i(\omega) = \frac{1}{U}\left|\sum_{n=0}^{M-1} x_i(n)w(n)e^{-j\omega n}\right|^2, i = 1,2 \ldots, M-1 \tag{7}$$

Where $I_i(\omega)$ is the periodogram of each segments, $w(n)$ refers to the window function in symmetric Hamming design [30], ω is the frequency and j is the imaginary unit. The U is the normalization factor that should satisfy the equation:

$$U = \frac{1}{M}\sum_{n=0}^{M-1} w^2(n) \tag{8}$$

Subsequently, the power spectrum of the signal is obtained by superposition and averaging according to Eq. (9).

$$P_x(e^j\omega) = \frac{1}{L}\sum_{j=1}^{L} I_i(\omega) \tag{9}$$

The data are, respectively, passed through two band-pass filters which correspond to the frequency range of breathing (frequency band of 0.1-0.5 Hz) and heartbeat (frequency band of 0.7-2.5 Hz). The band-pass filters are designed by using the "designfilt" function in the Matlab (R2020b). Then, the power spectrum of the signal is analyzed to find out the exact breathing and heartbeat frequency.

4. HR and BR monitoring

4.1. Pre-experiment test

The pre-test experiment was completed by using a stroboscopic light source (Shengwei Ltd., 10 mW) to simulate the steady changes of optical signal power caused by human breathing. The video was recorded for 20 seconds. As shown in Fig. 6, the experimental result indicates that optical power changes can be sensitively tracked by processing each image frame by frame and getting the sum of pixels. It has been shown that attenuation slightly increases with the temperature increase and slightly decreases with humidity increase [31-33]. Due to the fact that temperature and humidity do not change so much at room environment, their variations have weak effect on the performance of the sensor.

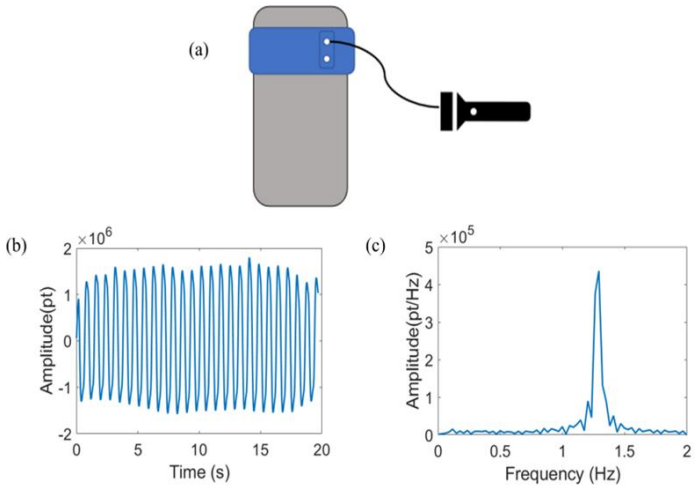

Fig.6. (a) Schematic diagram of the pre-experiment test; (b) Time-domain response of stroboscopic light source signal；(c) The power spectral density corresponding to the stroboscopic light source signal.

4.2. POF sensor for HR and BR monitoring

The POF is wrapped three times around the user's chest, where the sensing zone is aligned with the strongest heartbeat location. It is worth mentioning that wrapping three circles ensure that the POF fits the user's body stability and will be not loosen due to dynamic activities. Considering the variations of the performance of HR and BR, the video is recorded along four 30 s segments for a total of 2 minutes. The first experiment was implemented with one sensitivity zone, the original time-series data for 30 seconds as Fig. 7(a) shows, with MATLAB simulation we can obtain the breathing signal and heartbeat signal as Figs. 7(b) and (c) show. The frequency range of the signal indicates that we can obtain the breath signal clear, but the heartbeat signals are not as clear as shown in the inset of Fig. 7(d).

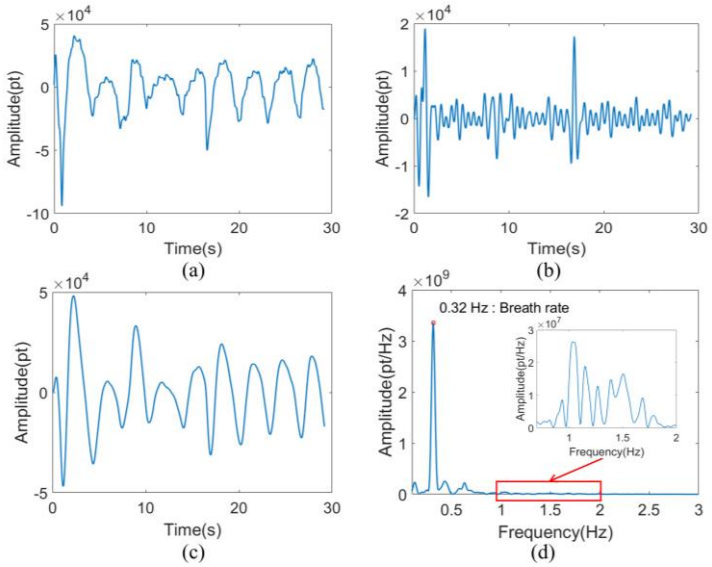

Fig. 7. Sensor with one sensitivity zone: (a) Original signal response in the time domain; (b) Breathing waveform; (c) Heartbeat waveform; (d) Signal response in the frequency domain (inset shows the detail around the frequency of 1.2 Hz)

The number of sensitivity zones may affect the HR and BR signal due to the amount of radiation leakage depending on the number of sensitivity zones. Besides, spatial multiplexing different sensitivity zones on the sensor can ensure sufficient signal leakage. In the following, we increase this number up to two and three in order to verify its impact on the HR and BR monitoring performance. The increased sensitivity zones are all on the same wrap, and considering the limited range of the apical impulse, the diameter of which is about 2.5 cm [34]. Considering the differences of each user's body, each zone is spaced 2 cm apart. Fig. 8 shows the experiment results with two sensitivity zones while the other parameters have been kept identical to previous measurements. From the original signal response in the time domain (see Fig. 8(a)), we can extract the information plotted in Figs. 8(b) and (c). Fig. 8(d) shows the frequency domain of the signal where the BR frequency is obtained as 0.34 Hz. However, from the inset of Fig. 8(d), the HR signal is still not strong enough to distinguish.

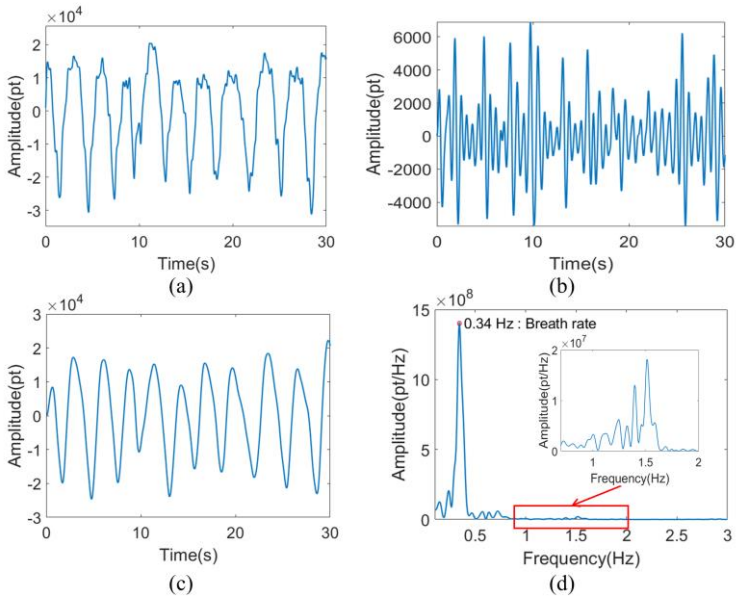

Fig. 8. Sensor with two sensitivity zones: (a) Original signal response in the time domain; (b) Breathing waveform; (c) Heartbeat waveform; (d) Signal response in the frequency domain.

Then, measurements were done with three sensitivity zones. In this case, the original time-domain signal is shown in Fig. 9(a). Figs. 9(b) and (c) present the time domain signal of breathing and heartbeat, respectively. As observed in Fig. 9(d), the BR and HR can be displayed in the power spectral density, which is 0.37 Hz and 1.56 Hz. It was repeated 5 times for each users. At the same time, BR was manually counted and HR was measured with a medical HR meter (CONTEC Ltd., CMS60D) for reference. Table 2 presents the measurement results and the comparison with the reference for HR and BR.

Table 2. The results of the POF sensor and the reference sensor for different subjects

Users	BR (bpm)		HR (bpm)	
	POF sensor	Reference	POF sensor	Reference
1	22.0±1.7	20.8±1.4	93.2±4.2	90.0±5.6
2	16.8±0.6	16.6±1.9	74.4±2.6	76.3±1.5
3	21.5±1.1	20.4±0.5	68.9±8.0	68.1±6.4
4	18.3±2.5	18.6±3.0	86.9±7.8	88.4±7.2

As presented in Table 2, the response indicate error lower than 5.8% for the BR measurements while 3.6% for the HR measurements. It indicates that the multiplexed POF sensor is effective in experiments to simultaneously measure breathing and heartbeat signals.

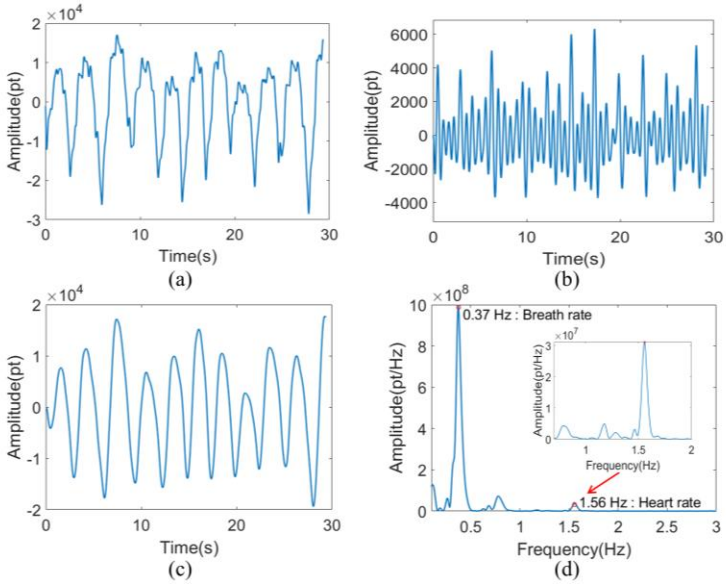

Fig. 9. Sensor with three sensitivity zones: (a) Original signal response in the time domain, (b) Breathing waveform, (c) Heartbeat waveform, (d) Signal response in the frequency domain.

4.3. Optimization of the smartphone system

The shutter speed determines the amount of light entering the camera's photosensitive components for each frame, which in turn affects each frame's sum of pixels. It can be seen from the previous discussion that the sum of the pixels acquired by the camera is a significant factor affecting the experimental results. Thus, an appropriate shutter speed needs to be defined.

The video was recorded for 3 minutes while the shutter speed was changed in steps of 30 seconds to obtain the highest amplitude of the power spectral density respectively: 30 s^{-1}, 60 s^{-1}, 120 s^{-1}, 240 s^{-1}, 480 s^{-1}, and 960 s^{-1}. The result shown in Fig.10 indicates that shutter speed has a negative correlation with the amount of light entering the camera.

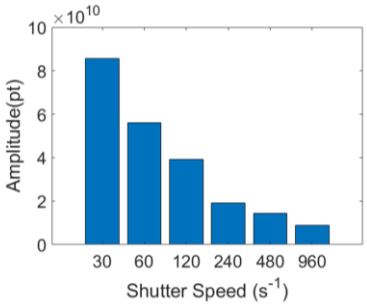

Fig. 10. The highest amplitude of the power spectral density at the different shutter speeds.

The original waveform and the extracted breathing waveform at different shutter speeds were acquired. As presented in Fig.11, the waveforms corresponding to the minimum (30 s^{-1}) and maximum (960 s^{-1}) shutter speeds were selected for comparison. Since the ambient light is mostly high frequency, at a high shutter speed, high-frequency ambient stray light will be captured by the camera, resulting in tiny irregular vibrations on the extracted breathing waveform. For this reason, the optimized shutter speed is set to the slowest 30 s^{-1} to reduce the interference of ambient light.

This shutter speed is sufficient to meet the needs of sensing sensitivity because the human HR is normally 1-2 beats/s.

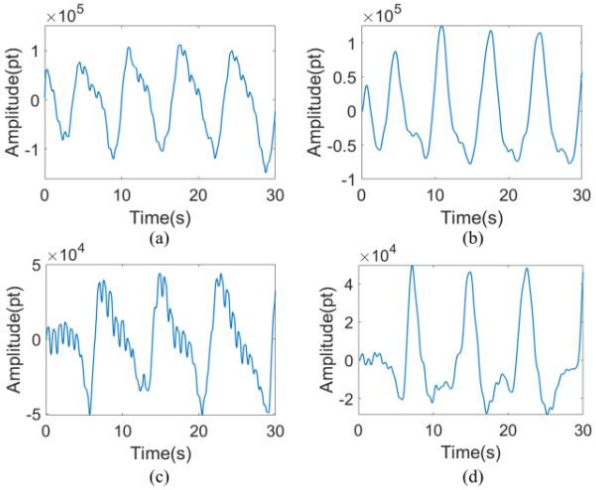

Fig.11. Original waveform and respiration with different shutter speeds: (a), (b) 30 s^{-1}; (c), (d) 960 s^{-1}, respectively.

4.4. Analysis of posture monitoring

The influence of different users' postures on the sensing was experimentally assessed. The sensor was fixed to the same position on the participant's chest to monitor the breathing and heartbeat activity of the participants in running, walking, standing, sitting and supine. Meanwhile, the participant was asked to stay in each posture for at least 2 minutes.

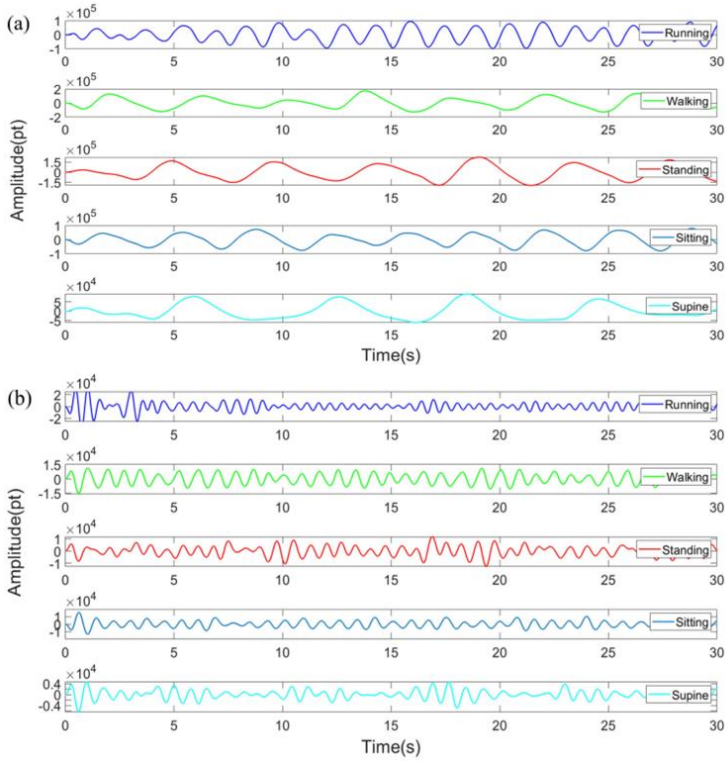

Fig. 12 (a) Breathing waveform at the different postures and (b) Heartbeat waveform at the different postures.

Data were recorded from each posture for 30 seconds to obtain the breathing waveform and the heartbeat waveform in different postures, as shown in Fig. 12. The result illustrates that the breathing and heartbeat waveforms extracted from different postures are obvious and

distinguishable, which indicates that the sensor can monitor the breathing and heartbeat activities of participants in various postures.

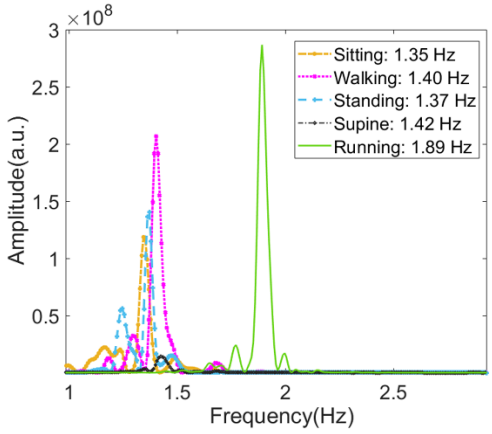

Fig. 13. Signal response in the frequency domain at the different postures.

Furthermore, the signal in the heartbeat band was collected for each posture, and the experiment was repeated and averaged. The extracted frequency domain of the heartbeat signal is shown in Fig. 13. For the same participant, the heart rate during running was 1.89 Hz, and the heart rate in other postures was similar around 1.38 Hz, which can be used to detect strenuous motion.

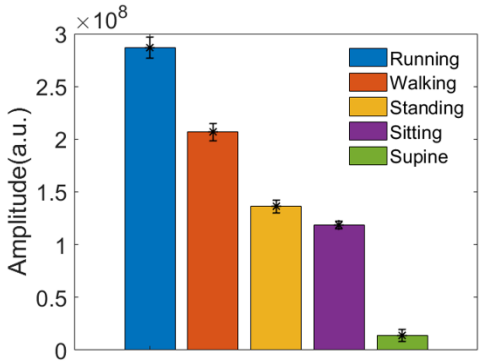

Fig. 14. The peak of the power spectrum in the heartbeat band in different postures.

The experimental result shows that the peak of the power spectrum in the heartbeat band can be used to differentiate and monitor body posture. As presented in Fig. 14, the spectral energy of the heartbeat band varies widely for different body postures, where the spectral energy in the dynamic state/activity (such as running) is much higher than that in the static state (such as supine). Specifically, the spectral energy is $2.8 \pm 0.11 \times 10^8$ pt during running and is $1.4 \pm 0.55 \times 10^7$ pt in the supine state. The spectral energies of walking, standing, and sitting were similar, with values is $2.0 \pm 0.84 \times 10^8$ pt, $1.4 \pm 0.61 \times 10^8$ pt, and $1.2 \pm 0.3 \times 10^8$ pt respectively.

5. Conclusion

This paper proposed and fabricated a POF-based integration for human physiological monitoring achieved by smartphone camera and flashlight. This device has the advantages of simplicity, low cost and it measures BR and HR at the same time. After the pre-experiment test to verify that optical power changes of POF are sensitive enough to be tracked by processing each

image frame by frame. The relationship between the number of sensing zones and the resolution of HR and BR signals is obtained. With three sensing zones we can obtain BR and HR clearly, at the same time, the shutter speed of the device is optimized, thus the relationship between shutter speed and the interference of ambient light is determined through analysis. The sensor presented here can monitor the HR and BR under different postures (running, walking, standing, squatting, and lying). There is a degree of positive correlation between the average optical power measured by the sensing device and the intensity of the movement, which means that it is possible to know the dynamic posture according to the analysis of spectral energy and frequency. The reported results have application prospects and commercial value for the field of intelligent wearable body feature detection.

Acknowledgments

This research was funded by National Natural Science Foundation of China (62003046,6211101138); Special Funds for the Cultivation of Guangdong College Students' Scientific and Technological Innovation (" Climbing Program" Special Funds) (pdjh2022a0684); Guangdong Provincial Department of Science and Technology(2021A1313030055); The Innovation Team Project of Guangdong Provincial Department of Education (2021KCXTD014); Special project in key field of Guangdong Provincial Department of Education (2021ZDZX1050); Guangdong Basic and Applied Basic Research Foundation (2021A1515011997).C. Marques acknowledges Fundação para a Ciência e a Tecnologia (FCT) through the CEECIND/00034/2018 (iFish project), PTDC/EEI-EEE/0415/2021 (DigiAqua) and this work was developed within the scope of the project i3N, UIDB/50025/2020 & UIDP/50025/2020, financed by national funds through the FCT/MEC.

References

[1] A. Al-Naji, K. Gibson, S.-H. Lee, J. Chahl, Monitoring of Cardiorespiratory Signal: Principles of Remote Measurements and Review of Methods, IEEE Access. 5 (2017) 15776–15790.

[2] X. Lin, S. Gao, T. Fei, S. Liu, H. Zhao, T. Zhang, Study on a paper-based piezoresistive sensor applied to monitoring human physiological signals, Sens. Actuat. A Phys. 292 (2019) 66–70.

[3] W. Li, Y. Yuan, J. Yang, L. Yuan, Review of Optical Fiber Sensor Network Technology Based on White Light Interferometry, Photonic Sens. 11 (2021) 31–44.

[4] C. Li, J. Tang, C. Cheng, L. Cai, M. Yang, FBG Arrays for Quasi-Distributed Sensing: A Review, Photonic Sens. 11 (2021) 91–108.

[5] R. Min, Z. Liu, L. Pereira, C. Yang, Q. Sui, C. Marques, Optical fiber sensing for marine environment and marine structural health monitoring: A review, Opt. Laser Technol. 140 (2021) 107082.

[6] P. Lu, N. Lalam, M. Badar, B. Liu, B.T. Chorpening, M.P. Buric, P.R. Ohodnicki, Distributed optical fiber sensing: Review and perspective, Appl. Phys. Rev. 6 (2019) 041302.

[7] R. Min, X. Hu, L. Pereira, M. Simone Soares, L.C.B. Silva, G. Wang, L. Martins, H. Qu, P. Antunes, C. Marques, X. Li, Polymer optical fiber for monitoring human physiological and body function: A comprehensive review on mechanisms, materials, and applications, Opt. Laser Technol. 147 (2022) 107626.

[8] A.G. Leal-Junior, C.A.R. Diaz, L.M. Avellar, M.J. Pontes, C. Marques, A. Frizera, Polymer Optical Fiber Sensors in Healthcare Applications: A Comprehensive Review, Sensors. 19 (2019) 3156.

[9] J. Guo, C. Yang, Q. Dai, L. Kong, Soft and Stretchable Polymeric Optical Waveguide-Based Sensors for Wearable and Biomedical Applications, Sensors. 19 (2019) 3771.

[10] C. Teng, R. Min, J. Zheng, S. Deng, M. Li, L. Hou, L. Yuan, Intensity-Modulated Polymer Optical Fiber-Based Refractive Index Sensor: A Review, Sensors. 22 (2021) 81.

[11] R. Min, L. Pereira, T. Paixao, G. Woyessa, X. Hu, P. Antunes, P. Andre, O. Bang, J. Pinto, B. Ortega, C. Marques, Chirped POF Bragg grating production utilizing UV cure adhesive coating for multiparameter sensing, Opt. Fiber Technol. 65 (2021) 102593.

[12] C. Markos, A. Stefani, K. Nielsen, H.K. Rasmussen, W. Yuan, O. Bang, High-T_g TOPAS microstructured polymer optical fiber for fiber Bragg grating strain sensing at 110 degrees, Opt. Express. 21 (2013) 4758.

[13] G. Woyessa, A. Fasano, A. Stefani, C. Markos, K. Nielsen, H.K. Rasmussen, O. Bang, Single mode step-index polymer optical fiber for humidity insensitive high temperature fiber Bragg grating sensors, Opt. Express. 24 (2016) 1253.

[14] G. Woyessa, A. Fasano, C. Markos, A. Stefani, H.K. Rasmussen, O. Bang, Zeonex microstructured polymer optical fiber: fabrication friendly fibers for high temperature and humidity insensitive Bragg grating sensing, Opt. Mater. Express. 7 (2017) 286.

[15] J.N. Dash, X. Cheng, D.S. Gunawardena, H.-Y. Tam, Rectangular single-mode polymer optical fiber for femtosecond laser inscription of FBGs, Photon. Res. 9 (2021) 1931.

[16] A. Theodosiou, R. Min, A.G. Leal-Junior, A. Ioannou, A. Frizera, M.J. Pontes, C. Marques, K. Kalli, Long period grating in a multimode cyclic transparent optical polymer fiber inscribed using a femtosecond laser, Opt. Lett. 44 (2019) 5346.

[17] R. Min, B. Ortega, A. Leal-Junior, C. Marques, Fabrication and Characterization of Bragg Grating in CYTOP POF at 600-nm Wavelength, IEEE Sens. Lett. 2 (2018) 1–4.

[18] C. Broadway, R. Min, A. Leal-Junior, C. Marques, C. Caucheteur, Towards commercial polymer fiber Bragg grating sensors: review and applications, IEEE/OSA Journal of Lightwave Technology, 37(1) (2019) 2605–2615.

[19]] L. Liu, J. Zheng, S. Deng, L. Yuan, C. Teng, Parallel Polished Plastic Optical Fiber-Based SPR Sensor for Simultaneous Measurement of RI and Temperature, IEEE Trans. Instrum. Meas.70 (2021) 9508308.

[20] L. Avellar, G. Delgado, C. Marques, A. Frizera, A. Leal-Junior, E. Rocon, Polymer Optical Fiber-Based Smart Garment for Impact Identification and Balance Assessment, IEEE Sensors J. 21 (2021) 20078–20085.

[21] P. Han, L. Li, H. Zhang, L. Guan, C. Marques, S. Savović, B. Ortega, R. Min, X. Li, Low-cost plastic optical fiber sensor embedded in mattress for sleep performance monitoring, Opt. Fiber Technol. 64 (2021) 102541.

[22] A.G. Leal-Junior, C.R. Díaz, C. Leitão, M.J. Pontes, C. Marques, A. Frizera, Polymer optical fiber-based sensor for simultaneous measurement of breath and heart rate under dynamic movements, Opt. Laser Technol. 109 (2019) 429–436.

[23] A. Aitkulov, D. Tosi, Optical Fiber Sensor Based on Plastic Optical Fiber and Smartphone for Measurement of the Breathing Rate, IEEE Sensors J. 19 (2019) 3282–3287.

[24] A. Aitkulov, D. Tosi, Design of an All-POF-Fiber Smartphone Multichannel Breathing Sensor With Camera-Division Multiplexing, IEEE Sens. Lett. 3 (2019) 1–4.

[25] 3D printer (Creality CR-3040 Pro), https://www.creality.com/goods-detail/creality-cr-3040-pro-3d-printer , access on 2022/03/03

[26] M. S.Kovacevic, A.Djordjevich, D. Nikezic, Analytical optimization of optical fiber curvature gauges. IEEE Sensors Journal 8 (2008) 227–232.

[27] S. E. Hayber, Analytical analysis and experimental validation of optical power estimation in V-grooved polymer optical fibers. Optik. 254 (2022) 168637.

[28] P. Antunes, J. Dias, T. Paixão, E. Mesquita, H. Varum, P. André, Liquid level gauge based in plastic optical fiber, Measurement. 66 (2015) 238–243.

[29] P. Welch, The use of fast Fourier transform for the estimation of power spectra: A method based on time averaging over short, modified periodograms, IEEE Trans. Audio Electroacoust. 15 (1967) 70–73.

[30] H. Jokinen, J. Ollila, O. Aumala, On windowing effects in estimating averaged periodograms of noisy signals,

Measurement. 28 (2000) 197–207.
[31] N. Zhong, Q. Liao, X. Zhu, M. Zhao, Y. Huang, R. Chen, Temperature-independent polymer optical fiber evanescent wave sensor, Scientific Reports, 5 (2015) 1-10.
[32] S. Savović, A. Djordjevich, Langevin Equation Approach to Mode Coupling in Heated Step-Index Plastic Optical Fibers. Journal of Russian Laser Research, 42 (2021) 154–160.
[33] S. Savović, M. S. Kovačević, J. S. Bajić, D. Z. Stupar, A. Djordjevich, M. Živanov, B. Drljača, A. Simović, K. Oh, Temperature dependence of mode coupling in low-NA plastic optical fibers, J. Lightwave Technol. 33, (2015) 89–94.
[34] D. H.Isaac, A. H. Levy, Position of the apex beat as a clinical sign. British Medical Journal. 1(1950) 349–351.